molecular pharmaceutics

Article

Cite This: Mol. Pharmaceutics 2018, 15, 2973−2983

Nitroxyl Modified Tobacco Mosaic Virus as a Metal-Free High-Relaxivity MRI and EPR Active Superoxide Sensor

Madushani Dharmarwardana,[†,#] André F. Martins,[†,⊥,#] Zhuo Chen,[†] Philip M. Palacios,[∥] Chance M. Nowak,[‡] Raymond P. Welch,[†] Shaobo Li,[†] Michael A. Luzuriaga,[†] Leonidas Bleris,[‡,§] Brad S. Pierce,[∥] A. Dean Sherry,[†,⊥] and Jeremiah J. Gassensmith*[,†,§]

[†]Department of Chemistry and Biochemistry, [‡]Department of Biological Sciences, [§]Department of Bioengineering, University of Texas at Dallas, 800 West Campbell Road, Richardson, Texas 75080-3021, United States

[∥]Department of Chemistry and Biochemistry, College of Sciences, The University of Texas at Arlington, Arlington, Texas 76019, United States

[⊥]Advanced Imaging Research Center, University of Texas Southwestern Medical Center, 5323 Harry Hines Boulevard, Dallas, Texas 75390, United States

Supporting Information

ABSTRACT: Superoxide overproduction is known to occur in multiple disease states requiring critical care; yet, noninvasive detection of superoxide in deep tissue remains a challenge. Herein, we report a metal-free magnetic resonance imaging (MRI) and electron paramagnetic resonance (EPR) active contrast agent prepared by "click conjugating" paramagnetic organic radical contrast agents (ORCAs) to the surface of tobacco mosaic virus (TMV). While ORCAs are known to be reduced in vivo to an MRI/EPR silent state, their oxidation is facilitated specifically by reactive oxygen species—in particular, superoxide—and are largely unaffected by peroxides and molecular oxygen. Unfortunately, single molecule ORCAs typically offer weak MRI contrast. In contrast, our data confirm that the macromolecular ORCA-TMV conjugates show marked enhancement for T_1 contrast at low field (<3.0 T) and T_2 contrast at high field (9.4 T). Additionally, we demonstrated that the unique topology of TMV allows for a "quenchless fluorescent" bimodal probe for concurrent fluorescence and MRI/EPR imaging, which was made possible by exploiting the unique inner and outer surface of the TMV nanoparticle. Finally, we show TMV-ORCAs do not respond to normal cellular respiration, minimizing the likelihood for background, yet still respond to enzymatically produced superoxide in complicated biological fluids like serum.

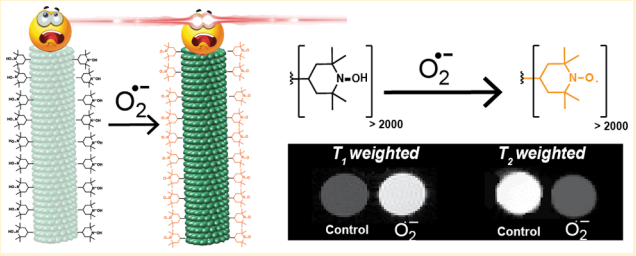

KEYWORDS: *tobacco mosaic virus, reactive oxygen species, magnetic resonance imaging, electron paramagnetic resonance, bioconjugation, organic radical contrast agents*

INTRODUCTION

The upregulation of reactive oxygen species (ROS), in particular, superoxide, is associated with certain cancers,[1,2] neurodegenerative disorders[1,3,4] such as Parkinson's disease,[5] diabetes,[6,7] mitochondrial diseases such as Friedreich ataxia,[8] Leber's hereditary optic neuropathy (LHON),[9] mitochondrial encephalomyopathy, lactic acidosis, stroke-like episodes (MELAS),[10] myoclonic epilepsy with ragged red fibers (MERRF),[11] and Leigh syndrome (LS).[3,4,12,13] The detection of superoxides, both extra and intracellularly, has consequently become an area of research interest in efforts to study and target diseased tissues.[14,15] Superoxide sensing in biological tissues has focused mainly on fluorescent imaging, as many dyes are easily quenched in the presence of ROS,[16,17] and superoxide in particular.[18] Moreover, the superoxides produced by people with diabetes can cause serious health complications such as heart injuries, and sensing of superoxide overproduction in these situations is also done using fluorescence imaging.[19,20] An unavoidable issue with fluorescence imaging in general, however, is limited tissue penetration, making it problematic for tissue imaging but ideal in guided surgery applications. Consequently, the need to detect cellular and biological events in deep tissue noninvasively has driven the development of "smart" probes for magnetic resonance imaging (MRI)[21−23] or electron paramagnetic resonance (EPR) modalities.[14,24] On the MRI front, paramagnetic chemical exchange saturation transfer (paraCEST) and other stimuli-responsive contrast agents have begun to generate considerable interest for their ability to detect changes in extracellular pH or production of specific

Special Issue: Click Chemistry for Medicine and Biology

Received: March 13, 2018
Revised: May 3, 2018
Accepted: May 17, 2018
Published: May 17, 2018

Downloaded via UNIV OF TEXAS AT DALLAS on April 19, 2021 at 15:12:50 (UTC).
See https://pubs.acs.org/sharingguidelines for options on how to legitimately share published articles.

© 2018 American Chemical Society

DOI: 10.1021/acs.molpharmaceut.8b00262
Mol. Pharmaceutics 2018, 15, 2973−2983

biological markers like lactate.[25−27] While redox active paraCEST agents based on lanthanides have emerged as potential sensors of singlet oxygen[28] and peroxide,[29] none have clearly emerged as candidates for superoxide.[25] Paramagnetic nitroxide organic radical contrast agents (ORCAs), on the other hand, have been making inroads toward superoxide detection in vivo and in vitro.[14,30−32] While sterically unencumbered nitroxide radicals like TEMPO (Figure 1b)

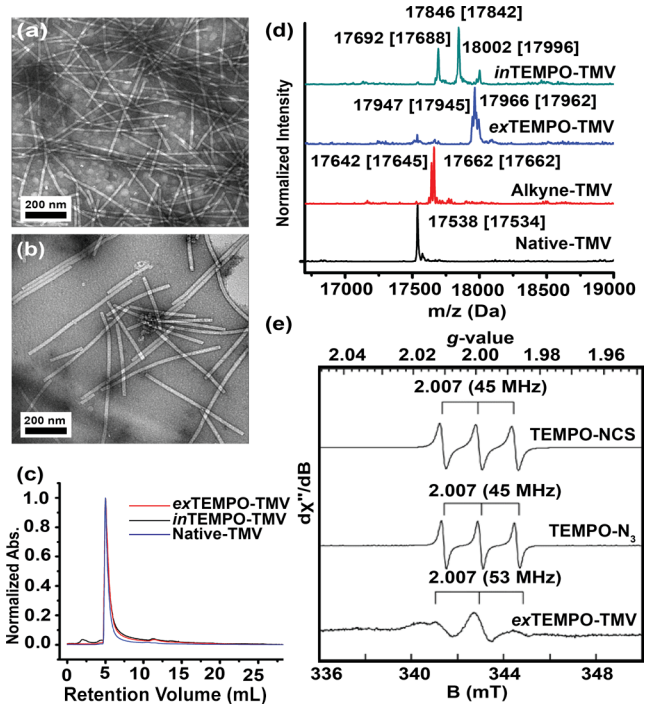

Figure 1. Characterization of TMV after bioconjugation reactions. The TEM images of (a) *ex*TEMPO-TMV and (b) *in*TEMPO-TMV shows the expected rod-like morphology. (c) A single peak in the SEC chromatogram (at 260 nm) of modified TMV confirms that the solution dispersity was unchanged. (d) Bioconjugation of the TEMPO radical to the TMV was characterized by ESI-MS. Native TMV has a peak at 17 538 m/z. The loss of this peak and emergence of a new peak at 17 662 m/z confirms that TMV was completely modified to alkyne-TMV. ESI-MS of *ex*TEMPO-TMV shows complete conjugation of TEMPO-N_3 to the alkyne-TMV. The peak at 17 966 m/z represents the attachment of the TEMPO radical to the TMV coat protein, whereas the peak at 17 942 m/z is the attachment of the TEMPO radical to the alkyne group with an unidentified elimination first noted by Francis (see ref 44) that has taken place during diazonium reaction. The interior surface of TMV consists of several glutamate residues, and three sites were modified via EDC coupling with TEMPO—one (17 692 m/z), two (17 846 m/z), or three (18 002 m/z) TEMPO molecules were installed. (e) X-band EPR spectra of *ex*TEMPO-TMV. The *ex*TEMPO-TMV sample was prepared in a capillary tube to minimize interaction between high dielectric aqueous solvent and the electric field of the incident microwave radiation.

are easily reduced to diamagnetic hydroxylamines in biological media, making their use as long-lived MRI contrast agents problematic, this property has been utilized to map redox activity in tumors ex vivo and in vivo.[33] On the other hand, reoxidation is kinetically favored by superoxide, while less reactive ROS, and in particular hydrogen peroxide, do not significantly oxidize hydroxylamines back.[1] Consequently, TEMPO can serve as a "turn-on" MRI sensor for superoxide. The benefit of "turn-on" over "turn-off" sensors is that they can have nearly infinite contrast against background.[34]

Nevertheless, ORCAs have historically suffered from low proton relaxation rates compared to metal-based contrast agents. These poor relaxivities have been cleverly addressed using polymeric systems,[33,35−39] as these multivalent scaffolds allow for high local concentrations of paramagnetic ORCAs. While such multimeric polymeric scaffolds allow for attachment of both MRI and fluorescence agents on the same platform, ORCAs are well-known and potent quenchers of adjacent fluorophores.[33] This quenching process means that when an ORCA is MRI/EPR active, adjacent fluorophores are typically quenched. While this has been elegantly exploited,[32,33,40,41] a true ratiometric sensor capable of assessing the probe concentration by fluorescence and the relative ROS levels by EPR/MRI signal would require a constant fluorescence emission regardless of the oxidation state of the ORCA.

Viral nanoparticles (VNPs) provide distinct structural features that make them well-suited to resolving some of these issues. For instance, they contain spatially well-defined functionalities, are rigid and monodisperse, and contain discrete topological surfaces that provide a distinct "outer" and "inner" surface.[42] These distinctions are well-suited for EPR active spin systems prone to spin pairing and relaxation when in close contact with other radical species.[25] Tobacco mosaic virus (TMV) is a 300 × 18 nm rod-shaped RNA virus that contains 2130 individual coat proteins.[43−45]

Each of these coat proteins contains an easily functionalizable tyrosine residue (Y139) on the exterior surface, which is spatially separated from the next closest accessible tyrosine[46] by 2.3−2.6 nm.[47,48] Furthermore, TMV contains a 4 nm narrow pore lined with glutamic acid residues (E97 and E106), likewise easily functionalized, and electronically inaccessible to the exterior surface.[49−51] These features provide two distinct advantages over existing polymeric nanostructures containing nitroxide radicals: (i) radical systems on the surface are spaced far enough apart so that spin−spin coupling is minimized even if 100% of the available functional groups are utilized, and (ii) fluorophores placed on the interior of the capsid will not be quenched by electron transfer processes from radical TEMPO moieties placed on the exterior surface. Previous studies have shown that VNPs and virus-like particles (VLPs) decrease the T_1 and T_2 relaxation times of attached metal-based MRI contrast agents.[41,48,52−63] The increase in r_1 ($1/T_{1p}$, p = paramagnetic contribution; $mM^{-1}{\cdot}s^{-1}$) relaxivity in these systems has been attributed to an increase in molecular diffusion and translation correlation times brought about by attachment to the surface of relatively massive, rigid, and slowly diffusing protein ensembles.

Here we present a method to create a sensitive EPR/MRI probe for superoxide detection in vitro with enhanced r_1 and r_2 relaxivities that rival clinically used molecular lanthanide-based MRI probes. The observed r_2/r_1 ratio allows TEMPO-conjugated TMV probes to operate as both a T_1 and T_2 contrast agent, making these probes valuable for both clinical (<3 T) and preclinical (>3 T) MRI scanners. We have also designed a bimodal TEMPO-TMV probe for ratiometric fluorescence experiments that is functionalized with a fluorescent dye on the interior and with an ORCA for MRI/EPR imaging on the exterior. The unique topology of the VNP scaffold allows for the insertion of an internal fluorescent probe as a concentration marker that is insensitive to the oxidation

DOI: 10.1021/acs.molpharmaceut.8b00262
Mol. Pharmaceutics 2018, 15, 2973−2983

Scheme 1. (a) Representations of a Single TMV Nanoparticle[a] and a Single TMV Coat Protein Highlighting Solvent Exposed Amino Acid Residues Available for Bioconjugation Reactions, (b) Oxidation States of Nitroxide Radicals,[b] (c) Bioconjugation to the Interior Surface of TMV via EDC Coupling Reaction To Make *in*TEMPO-TMV, and (d) TMV Bioconjugation on the Exterior via Stepwise Diazonium Coupling Followed by a CuAAC Reaction To Make *ex*TEMPO-TMV

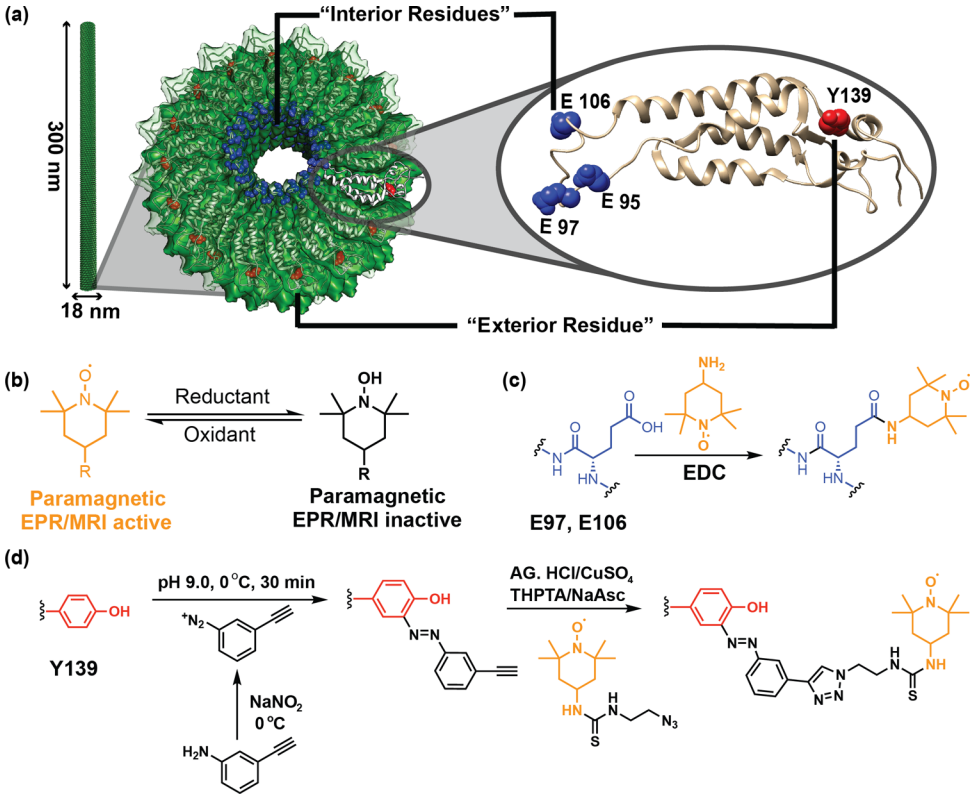

[a]Created in Chimera using PDB ID of 2tmv. [b]Paramagnetic radical species can be detected by both EPR and MRI, whereas the reduced diamagnetic species is neither MRI nor EPR active.

state of the ORCA probe. Finally, we present the evaluation of these probes in both cells and serum.

RESULTS AND DISCUSSION

Attaching ORCA to the Surfaces of TMV. As shown in Scheme 1a, TMV contains two distinct surfaces: (i) an outer surface with few charged functional groups and uninhibited access to bulk water and (ii) a 4 nm narrow inner channel with a net negative surface charge and less access to diffusing bulk water. We thus first set to determine if there would be any difference in measured relaxivities if ORCAs were placed on the inner vs the outer surface of TMV. The interior surface of TMV contains solvent exposed glutamic acid residues, which we functionalized via EDC coupling with TEMPO-NH_2 (Scheme 1c). High-performance liquid chromatography/electron spray ionization mass spectroscopy (HPLC/ESI-MS) confirms that three sites were modified following the EDC coupling reaction to yield *in*TEMPO-TMV. As shown in Figure 1d, peaks at 17 692 Da, 17 846 Da, and 18 002 Da represent the attachment of one, two, and three molecules of TEMPO, respectively, to the coat protein monomers of TMV. While only glutamate residues E97 and E106 have been identified as reactive sites,[49] the third peak at 18 002 Da likely corresponds to E95. Though three conjugations to this inner channel have been observed[55] before, the residue of the third modification site has never been identified. Separately, the exterior surface of TMV was functionalized initially using a diazonuim coupling reaction[49] (alkyne-TMV) with in situ prepared 3-ethynylphenyldiazonium salt. This quantitative reaction was followed by a copper-catalyzed azide−alkyne cycloaddition[64] (CuAAC) with TEMPO-N_3 to yield *ex*TEMPO-TMV (Scheme 1d).

The TEMPO radical is known to be reduced in the presence of sodium ascorbate, so we modified a procedure initially described by Finn[65] by forming Cu^I(THPTA) separately by mixing a 1:5:1 molar ratio of Cu^{II} sulfate, the ligand THPTA, and sodium ascorbate in water. Starting with Cu^{II} sulfate as opposed to directly using a Cu^I source to form the Cu^I(THPTA) complex provided consistently high yields, likely because of the more favorable aqueous solubility of Cu^{II} sulfate. This solution was transferred quickly in open air to an aqueous solution of TMV under N_2. Degassing of solutions were not necessary, and the successful attachment of the new functional groups was again confirmed by HPLC/ESI-MS. As shown in Figure 1d, after the quantitative diazonium coupling reaction, all of the TMV coat protein monomers were modified to the azo adduct (17 666 Da) in line with previous literature reports.[66] The CuAAC reaction on the alkyne-TMV with TEMPO-N_3 proceeded quantitatively, evidenced by the loss of the alkyne peak at 17 666 Da. The morphology and dispersity of TMV were checked after each bioconjugation reaction and were found unchanged by transmission electron microscopy (TEM) and size exclusion chromatography (SEC), respectively (Figures 1a−c and S11).

Finally, EPR spectroscopy was used to characterize the presence of paramagnetic species on the TMV surface. As shown in the Figure 1e, small molecule TEMPO radicals

DOI: 10.1021/acs.molpharmaceut.8b00262
Mol. Pharmaceutics 2018, 15, 2973−2983

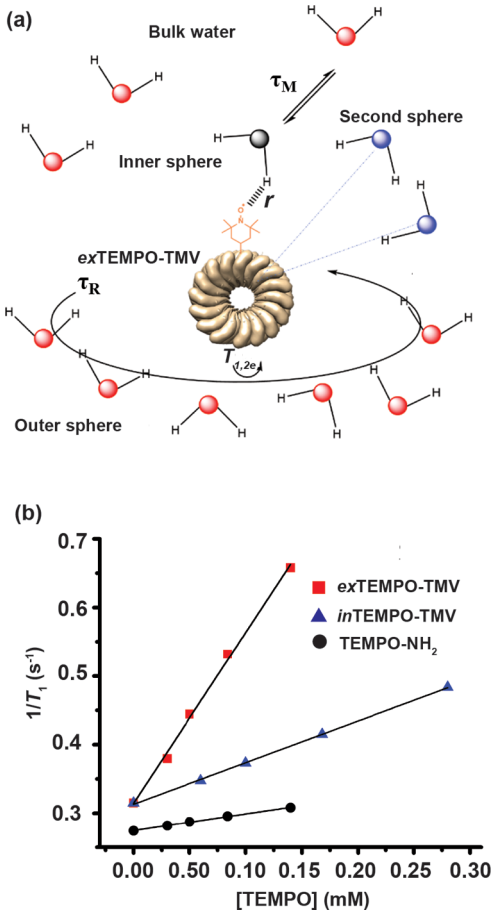

Figure 2. (a) Schematic representation of the *ex*TEMPO-TMV with one coordinated water molecule (inner-sphere water, its oxygen is colored black) in solution (bulk water, oxygens are red). Second-sphere water molecules (water oxygens are blue). The parameters that govern the relaxivity are also represented: NO−H distance (r), the mean lifetime (τ_m) of the water molecule(s) in the inner sphere, the rotational correlation time (τ_R), and the electronic spin relaxation times (T_{1e} and T_{2e}). (b) Plot of $1/T_1$ (s^{-1}) versus TEMPO concentration (mM) for *ex*TEMPO-TMV, *in*TEMPO-TMV, and TEMPO-NH_2 at 23 MHz in 0.1 M pH 7.4 KP buffer and 310 K.

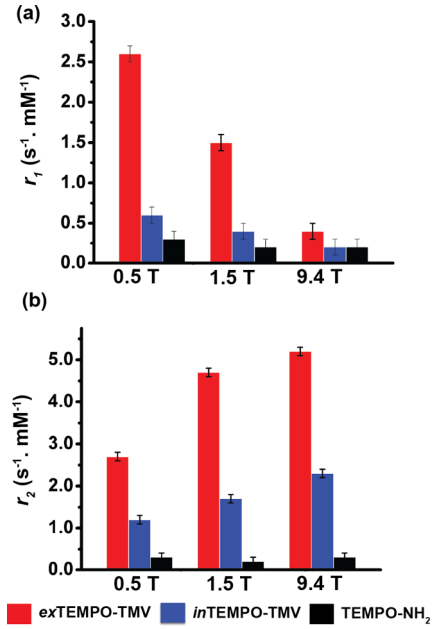

Figure 3. Determined (a) r_1 and (b) r_2 relaxivities for the agents *ex*TEMPO-TMV, *in*TEMPO-TMV, and TEMPO-NH_2 at different fields in 0.1 M pH 7.4 KP buffer and 310 K.

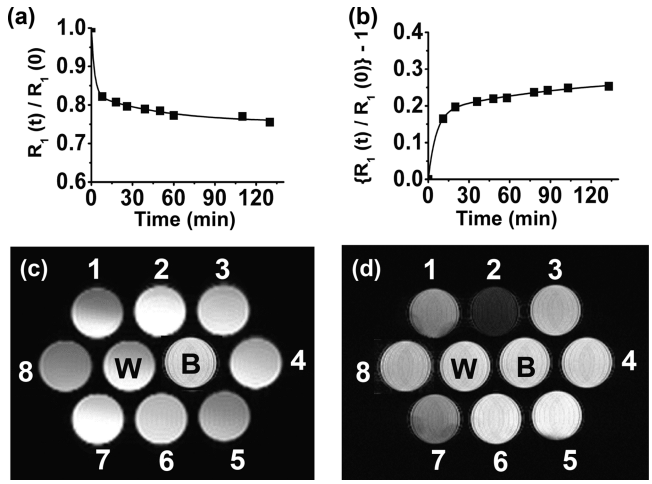

Figure 4. (a) Evolution of the relative water proton paramagnetic relaxation rate of a 0.14 mM aqueous solution of *ex*TEMPO-TMV in the presence of 100-fold molar excess of ascorbate. Plot normalized to the initial value $R_1^{(t)}/R_1^{(0)}$ as a function of the time (min) and measured at 23 MHz, 0.1 M pH 7.4 KP buffer, 310 K. (b) Evolution of the relative water proton paramagnetic relaxation rate of a 0.14 mM aqueous solution of *ex*TEMPO-TMV (reduced) in the presence of 100-fold molar excess of KO_2. Plot normalized to $(R_1^{(t)}/R_1^{(0)} - 1)$ as a function of the time (min) and measured at 23 MHz, 0.1 M pH 7.4 KP buffer, 310 K. The solid lines through the data points represent the pseudo-first-order reaction fits. (c) T_1-weighted and (d) T_2-weighted fast spin−echo images (TE = 200 ms) of (1) *ex*TEMPO-TMV oxidized with KO_2, (2) *ex*TEMPO-TMV (0.14 mM/TEMPO), (3) *ex*TEMPO-TMV reduced with ascorbate, (4) ascorbate in PBS, (5) TEMPO-NH_2 (1.4 mM), (6) TEMPO-NH_2 (0.14 mM), (7) *in*TEMPO-TMV (0.14 mM/TEMPO), (8) KO_2 in PBS, (W) water at pH 7.0, (B) PBS buffer at pH 7.0 taken at 9.4 T and 293 K.

showed a characteristic ^{14}N-triplet (I = 1; A ∼ 45 MHz) centered at a g-value of 2.007, which is typical of the nitrogen-centered radical. The sharp line width and isotropic g/A-values are consistent with rotational averaging. By contrast, the *ex*TEMPO-TMV (Figure 1e) and *in*TEMPO-TMV (Figure S12) results in significantly broader and more anisotropic EPR spectra. The distributed g/A-values and attenuated signal intensity are attributed to decreased rotational and translational mobility of the radical. This significantly increases the observed line width of the mobilized radical. High density of radicals can also result in dipolar spin−spin exchange, which also contributes to the increased line width.

Proton Relaxation Properties of ORCA Loaded TMV Rods. To characterize the relaxation behavior of the TEMPO-TMV particles, we performed proton relaxometric measurements at different fields. It is worth noting that nitroxide radicals normally bind noncovalently to at least one water molecule,[67] which is similar to that found with metal-based complexes with one or more water molecules coordinated to the inner sphere of the metal centers.[34,68] The overall proton relaxation behavior is determined by the sum of the inner-sphere and outer-sphere contributions.[34] While the outer-sphere contributions cannot be neglected, the inner-sphere contributions are typically dominant.[69] For nitroxide radicals, under the extreme narrowing condition,[70,71] the primary inner-

DOI: 10.1021/acs.molpharmaceut.8b00262
Mol. Pharmaceutics 2018, 15, 2973−2983

Scheme 2. (a,b) *in*FITC-*ex*TEMPO-TMV Bimodal Imaging Probe and (c) Diagram of TMV Showing the Relative Placement of the Fluorescent Dye on the Interior Residues and the ORCAs on the Exterior[a]

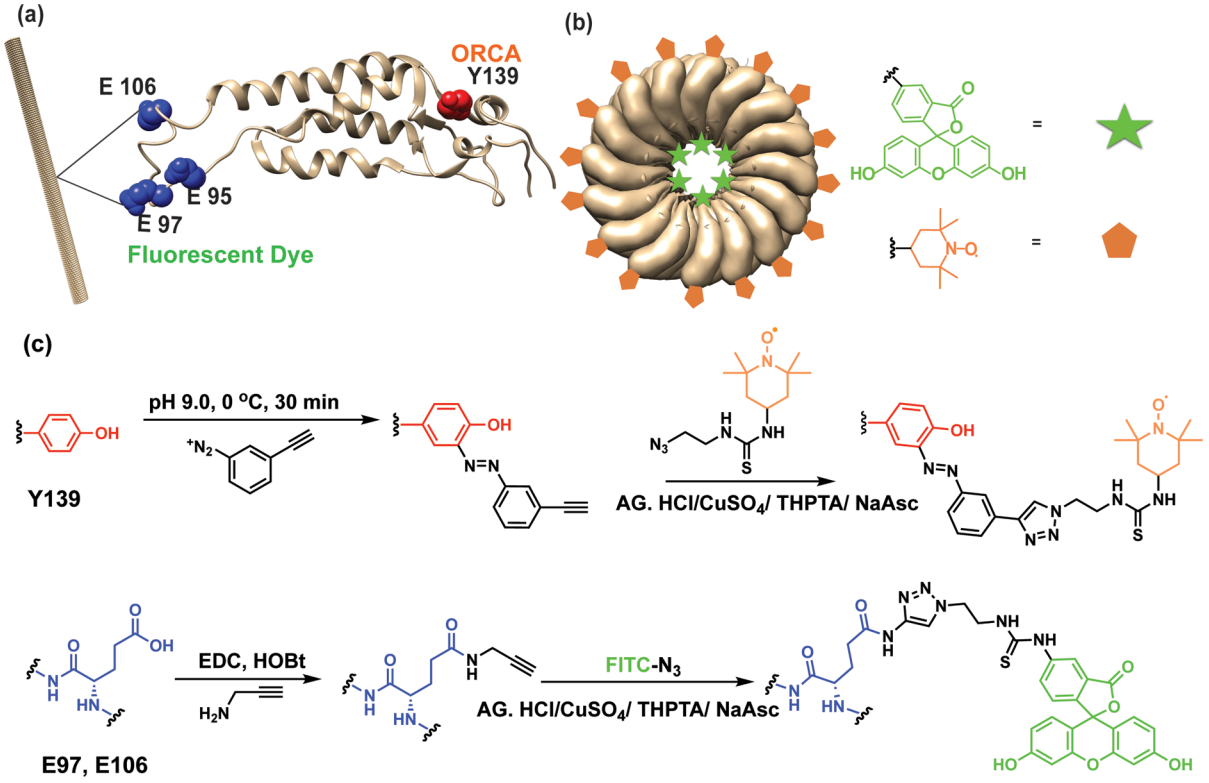

[a]The exterior surface was first modified with TEMPO radicals via diazonium coupling followed by a CuAAC reaction, and then, the interior surface of TMV was modified by EDC coupling with propargylamine followed by a CuAAC reaction.

sphere relaxation mechanism is determined by dipolar and Curie dipolar contributions.[72,73] However, at higher magnetic fields, line broadening predominantly originates from Curie spin relaxation processes. The dipolar and Curie mechanisms from the inner- and outer-sphere contributions can be modeled as described in previous detailed reports.[73−75] Large macromolecules, like the TMV presented here, are characterized by slow rotation dynamics in solution[33,35] commonly represented by the rotational correlation time (τ_R). Other factors that have a high impact on the relaxation processes for T_1 and T_2 are the electronic relaxation rates ($1/T_{ei}$; i = 1, 2) and solvent exchange lifetimes (τ_m) as defined by the correlation times (τ_{ci}; i = 1, 2)

$$\tau_{ci} = \frac{1}{T_{ei}} + \frac{1}{\tau_m} + \frac{1}{\tau_R}, \; i = 1, 2 \qquad (1)$$

We can make several simplifying assumptions. In systems where T_e is short, as is the case of TEMPO radicals ($T_{ei} \geq 20$ ns),[39] the molecular rotation and water exchange dominate τ_{ci}.The water exchange rate ($k_{ex} = 1/\tau_m$) for nitroxide radicals has been estimated to be quite slow ($k_{ex} \sim 2 \times 10^{-4}$ s),[39] and it is expected from theory[76] that the low-field total transverse relaxivity (T_2) will be small and similar to the longitudinal relaxivity, since it is modulated by T_e. At higher magnetic fields, the r_2 relaxivity is mostly affected by the square of the field (not r_1) and increases with field strength. As shown in Table S2, *ex*TEMPO-TMV, the most efficient system (Figure 2b), shows a significant increase in r_2 at 9.4 T to 5.2 s^{-1} mM^{-1} per TEMPO compared to lower fields where r_1 and r_2 were similar.

Our data show that the TEMPO-TMV conjugates are efficient T_1 and T_2 contrast agents at low field and present remarkable properties as T_2 agents at high field,[35] with the greatest enhancement seen for *ex*TEMPO-TMV (Table S2). Indeed, *ex*TEMPO-TMV shows an enhancement of r_1 and r_2 at low field nearly 1 order of magnitude higher than that of the corresponding small molecule TEMPO-NH_2, and at high-field, the r_2 shows a 13-fold increase compared to that of TEMPO-NH_2. A comparison of $r_1$and r_2 values for *ex*TEMPO-TMV and *in*TEMPO-TMV (Figure 3a,b) show that the exterior functionalization yields higher relaxivity values at all fields and both r_1 and r_2 relaxivities compare very favorably to existing polymeric ORCAs and small molecule contrast agents (Table S3).These data suggest that the TEMPO spins located on the inner cavity of the TMV macromolecule may have less access to bulk water preventing optimal exchange between the inner-sphere water molecules and those in the close vicinity of the TEMPO spin.[77]

Nitroxide-based ORCAs typically undergo rapid reduction to diamagnetic hydroxylamines in the presence of reducing agents such as ascorbate.[78,79] Relaxometric studies of *ex*TEMPO-TMV, shown in Figure 4a, confirm that, in the presence of an equimolar amount of ascorbate, about 20% of the paramagnetic TEMPO spins on the *ex*TEMPO-TMV are reduced within a few minutes. This was also confirmed by EPR spectroscopy (Figure S13a). As proof of principle that TEMPO-TMV compounds could be used as potent indicators of strong ROS, we performed the relaxometric experiments over the same time span, but in the presence of an excess of KO_2 at 0.4 T. In this case, the T_1 of water protons recovered to nearly the original values (Figure 4b). This same reoxidation experiment was confirmed using EPR spectroscopy (Figure S13b).We inves-

DOI: 10.1021/acs.molpharmaceut.8b00262
Mol. Pharmaceutics 2018, 15, 2973−2983

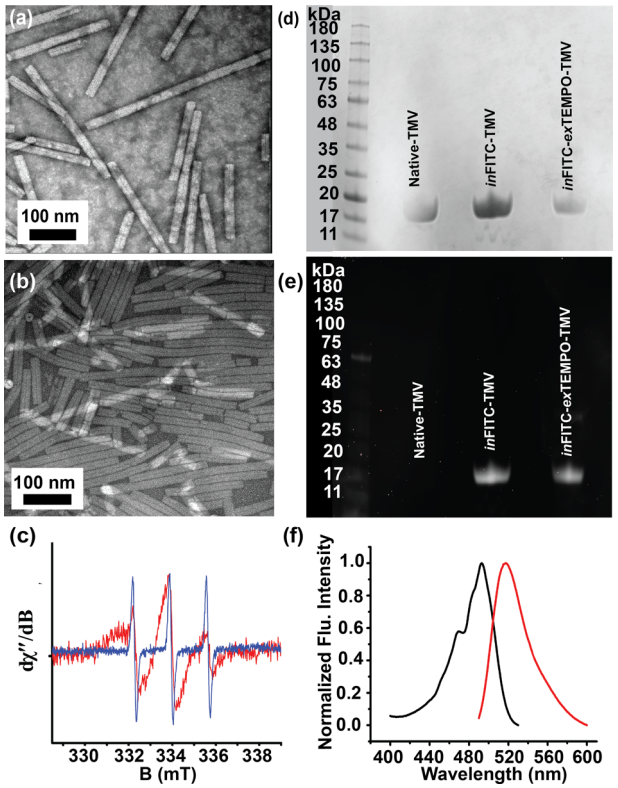

Figure 5. Synthesis and characterization of *in*FITC-*ex*TEMPO-TMV; TEM images: (a) *in*FITC-TMV, (b) *in*FITC-*ex*TEMPO-TMV. (c) EPR spectrum of *in*FITC-*ex*TEMPO-TMV (red) and TEMPO-NH_2 (blue). SDS-PAGE to confirm that FITC has been successfully attached to TMV; SDS-PAGE was visualized by (d) Coomassie brilliant blue and (e) UV. (f) Excitation (black line) and emission (red) spectra of *in*FITC-*ex*TEMPO-TMV.

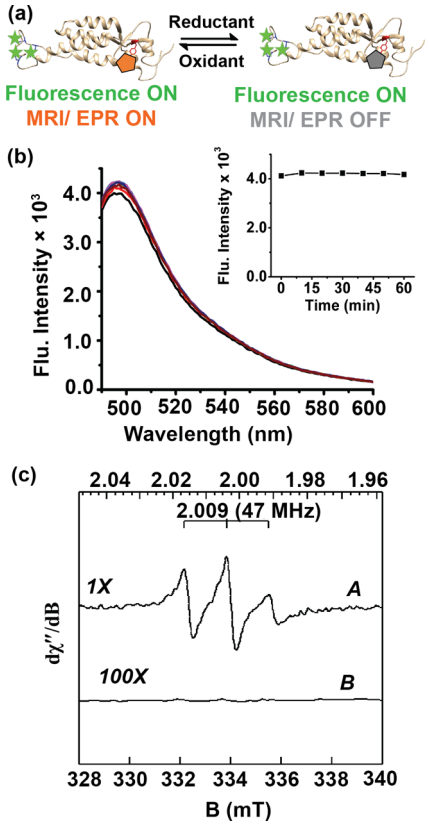

Figure 6. Bimodal imaging characteristics of the *in*FITC-*ex*TEMPO-TMV redox probe. (a) Protein crystal structure of a single coat protein of TMV showing the attachment of FITC and TEMPO to the inner (glutamate) and outer (tyrosine) surfaces, respectively. (b) Time-dependent emission behavior of *in*FITC-*ex*TEMPO-TMV redox probe upon addition of 100 eq of ascorbate in 0.1 M pH 7.4 KP buffer. (c) EPR spectra of *in*FITC-*ex*TEMPO-TMV redox probe before (A) and 60 min after (B) addition of 100 eq of ascorbate in 0.1 M pH 7.4 KP buffer. An identical experiment on Cy5 was conducted, and details are in Figure S13.

tigated the rate of reduction of the *ex*TEMPO-TMV under pseudo-first-order conditions using a 100-fold excess of ascorbate in pH 7.4 phosphate-buffered saline (PBS). Fits were obtained for relaxometric data collected over a 2 h period. Pseudo-first-order rate constants, k', were obtained by following the decay of the $R_1^{(t)}/R_1^{(0)}$ determined by proton relaxometry. Excellent agreement with literature values was found for *ex*TEMPO-TMV and other macromolecules ($k' = 17 \times 10^{-4} \pm 0.1\ s^{-1}$) as shown in the Table S4.[33,35,39] Conversely, the oxidation of the reduced *ex*TEMPO-TMV hydroxylamine with an excess of KO_2 also showed a quite extensive reaction with a $k' = 16 \times 10^{-4} \pm 0.1\ s^{-1}$.

In Vitro MR Imaging. In support of these experimental observations, we have performed phantom imaging on several samples containing *ex*TEMPO-TMV, *in*TEMPO-TMV, reduced *ex*TEMPO-TMV, oxidized *ex*TEMPO-TMV, and standards. T_2-weighted MR imaging at 9.4 T showed that among the 10 tubes, only those containing the nonreduced TMV-TEMPOs showed enhanced T_2 contrast, whereas the free TEMPO (Figure 4d, wells 5 and 6) do not show any contrast difference even when we doubled the concentration of free TEMPO sample (Figure 4d, well 6). While contrast enhancement is evident in the T_1-weighted images (Figure 4c, wells 8 vs 2), the greatest contrast at this field strength comes from the T_2-weighted images (Figure 4d, wells 8 vs 2).These results suggest that these TEMPO macromolecular derivatives can detect changes in superoxides at millimolar concentrations. It also shows the potential of using *ex*TEMPO-TMV as a high-field (T_2) contrast agent. This is particularly relevant, because most of clinical MR scanners operate at low fields (0.4−3 T), though implementation of clinical high-field scanners is progressing.

***in*FITC-*ex*TEMPO-TMV for Bimodal Molecular Imaging.** After confirming that *ex*TEMPO-TMV exhibits better T_1 and T_2 relaxation characteristics compared to *in*TEMPO-TMV, this compound was used for all additional studies. A second goal of using TMV as a platform was to install a fluorophore for bimodal imaging in a position where it would not be quenched by the TEMPO radicals (Scheme 2). The order of the bioconjugation reactions to the TMV virus surface is important to minimize the redox chemistry on the attached TEMPO. We first functionalized the interior surface with FITC using standard CuAAC conditions and then functionalized the exterior surface with TEMPO radicals using our modified procedure. After each bioconjugation reaction, the integrity of the particle was characterized by SEC and TEM (Figure 5a,b). Moreover, TEMPO radical attachment to the exterior surface was confirmed by EPR spectroscopy (Figure 5c). The attachment of FITC to the interior surface of TMV was confirmed by UV−vis spectroscopy (Figure S14), SDS-PAGE (Figure 5d,e), and fluorescence spectroscopy (Figure 5f). To show this quenching process is not dependent on FITC, we

DOI: 10.1021/acs.molpharmaceut.8b00262
Mol. Pharmaceutics 2018, 15, 2973−2983

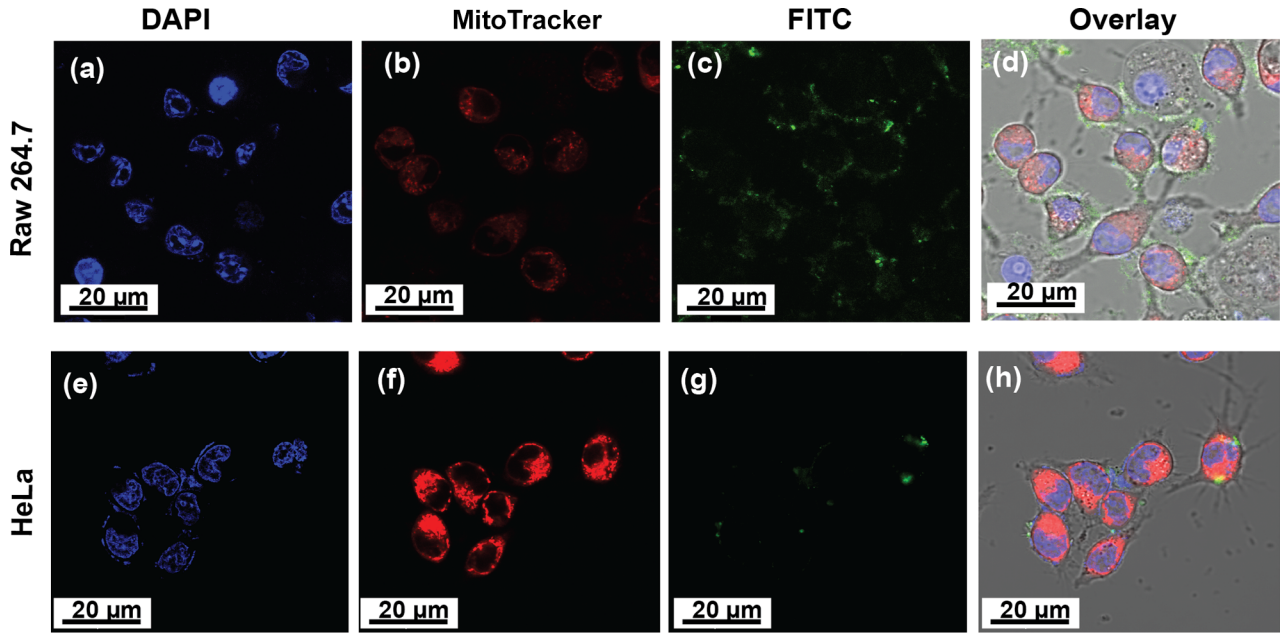

Figure 7. Confocal microscopy images of cellular uptake of *in*FITC-*red-ex*TEMPO-TMV redox probe with (a–d) RAW 264.7 cells and (e,f) HeLa cells. Color code: blue, Hoechst 33342; red, MitoTracker Deep Red; green, *in*FITC-*red-ex*TEMPO-TMV.

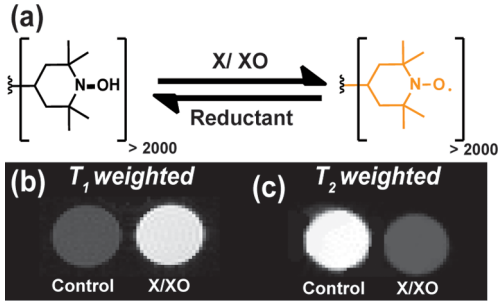

Figure 8. (a) Schematic showing the redox behavior of *red-ex*TEMPO-TMV. (b) T_1-weighted phantom images and (c) T_2-weighted phantom images before and after addition of X/XO. The concentration of TMV sample was 5.0 mg mL^{-1}, and the reaction mixture consisted of 50% of serum by volume.

attached a cyanine dye (Cy 5) to the interior as well, and we again observed minimal quenching from the radical (Figures S15–S17).

Fluorescein and cyanine dyes, like most fluorophores, are known to be quenched by nitroxyl radicals,[33,42,80] and the tube-like architecture of TMV allowed us to attach the MRI imaging agent and the fluorescent dye far enough apart to prevent quenching of the fluorescence emission of the dye (Figure 6a). To our satisfaction, we found less than 3% variation in fluorescence when shifting between the oxidized radical to the reduced hydroxylamine (Figure 6b) even after an hour following addition of 100 eq of ascorbate. On the other hand, the EPR spectra (Figure 6c) confirms that the radicals are completely reduced by the ascorbate under these same conditions. We again conducted the same experiment with *in*Cy5-*ex*TEMPO-TMV and confirmed that the oxidation state of the radical does not affect the emission intensity of Cy 5 (Figure S18), showing the generalizability of this approach with different dyes.

In Vitro-*in*FITC-*red-ex*TEMPO-TMV Studies. While the ultimate goal is in vivo imaging, in these early studies, we found it important to ascertain their behavior in cells and in serum. Cellular uptake could potentially result in trafficking to organelles normally high in superoxide concentrations, such as mitochondria, and could create an unwanted background signal. Further, uptake by macrophages, which are known to efficiently remove macromolecules and nanoparticles, could potentially reduce the circulatory half-life of these particles and may lead to the formation of antibodies against our probe making their clearance faster.

Studies have shown that macrophages as well as HeLa cells interact less effectively with high aspect ratio nanoparticles, and TMV in particular has been extensively studied.[52,81,82] We were curious if we would see uptake with reduced *in*FITC-*ex*TEMPO-TMV (*in*FITC-*red-ex*TEMPO-TMV) nanoparticles and if this would cause changes in the oxidation state of the ORCA following uptake. We used confocal microscopy on our "quenchless" system to investigate the interaction between *in*FITC-*red-ex*TEMPO-TMV and macrophages. The confocal microscopy data shows that *in*FITC-*red-ex*TEMPO-TMV (Figure 7d) associates with macrophages by adhering to the surface with no obvious fluorescence inside the cells and, in particular, the mitochondria, which are stained red in Figure 7b. We also investigated the cellular uptake of *in*FITC-*red-ex*TEMPO-TMV by HeLa cells (Figure 7e–g) and found no significant fluorescence signal coming from cells (Figure 7g). The lack of interaction with mitochondria was corroborated by EPR spectroscopy. To ensure we would observe signal if any trafficking to mitochondria occurs at all, we stimulated the HeLa and macrophages with the superoxide promotor phorbol 12-myristate 13-acetate (PMA)[83−85] and then incubated these cells with *red-ex*TEMPO-TMV for an hour. Cells were collected, and EPR spectra were recorded as a function of time. A lack of an EPR signal over time confirms that *red-ex*TEMPO-TMV has not been uptaken by cells (Figure S21). If the *red-ex*TEMPO-TMV had been taken up by the cells and trafficked to an area of ROS activity, we would expect to observe an increase in the EPR signal intensity with time, particularly when the cells were stimulated by PMA.[83] These

DOI: 10.1021/acs.molpharmaceut.8b00262
Mol. Pharmaceutics 2018, 15, 2973−2983

results are promising as it suggests that background signal from cellular metabolism is minimal.

***red-ex*TEMPO-TMV Performance in Serum.** Serum is very rich in a variety of proteins that may interfere with superoxide detection either by (i) directly reducing TEMPO to its EPR silent form or (ii) by covering the probe with a layer of protein—commonly called a protein corona—which would inhibit the "turn-on" response. To ascertain if our sensor functions in a biological environment, which might mimic detection of superoxide from tissue damage, for instance, we tested *red-ex*TEMPO-TMV in serum solution using enzymatically produced superoxide. Xanthine/xanthine oxidase (X/XO) was employed as a superoxide generating agent, as it has been shown[86,87] to be a good model of cell-free superoxide generation via EPR/MRI.[1] First, the *red-ex*TEMPO-TMV was made by reduction of *ex*TEMPO-TMV with 0.1 M sodium ascorbate in a suspension of PBS, which was then purged with nitrogen gas to prevent reoxidation. Xanthine (final concentration of 0.05 mM) and *red-ex*TEMPO-TMV (final concentration of 5.0 mg mL^{-1}) were mixed in fetal bovine serum (FBS). Finally, xanthine oxidase (final concentration of 0.1 U/mL) was added to the mixture. EPR spectra were recorded over 24 h, and MR phantom images were obtained from the same samples. Reoxidation of the probe was evident immediately. The T_1-weighted images and T_2-weighted images for the *red-ex*TEMPO-TMV sample with and without X/XO shows a huge contrast difference (Figure 8b,c) clearly indicating that the serum did not prevent detection of superoxide. These changes were confirmed by EPR, which also showed the regeneration of the TEMPO radical by the superoxide formed from X/XO (Figure S22) in the serum solution.

CONCLUSIONS

This was a fundamental study of the synthesis, magnetic, and optical characterizations, and in vitro analyses of a new type of a fluorescent/MRI active superoxide sensor that works at both high and low magnetic fields. Our ORCA-conjugated VNP-based nanoparticle probe appears promising for use at both clinical (<3 T) and preclinical (>3 T) MRI fields. Attachment of ORCA to TMV rods resulted in a 10-fold increase in r_1 and a 13-fold increase in r_2 compared to that of the small molecule ORCAs. We have proposed that these increases in relaxivity are ascribed to a decrease in the molecular rotation and diffusional motions brought about by attachment of the ORCA to the large rod-shaped particle. The distinct "inner" and "outer" topology of the TMV permits the creation of a "quenchless" ORCA-based bimodal probe for combined MRI and fluorescence imaging. The probe shows "turn-on" functionality toward enzymatically produced superoxide in the presence of serum, yet does not show appreciable changes in EPR intensity even when endocytosed by cells, suggesting this probe would be ideal for imaging diffuse tissue injury as may be the case in deep tissue diabetic ulceration or coronary heart disease.

ASSOCIATED CONTENT

Supporting Information

The Supporting Information is available free of charge on the ACS Publications website at DOI: 10.1021/acs.molpharmaceut.8b00262.

Detailed experimental and synthetic procedures and characterization of small molecules, TMV isolation and purification protocols, bioconjugation protocols, electron paramagnetic studies, instrumentation (PDF)

AUTHOR INFORMATION

Corresponding Author

*E-mail: gassensmith@utdallas.edu.

ORCID

Madushani Dharmarwardana: 0000-0002-3086-047X
Michael A. Luzuriaga: 0000-0001-6128-8800
Jeremiah J. Gassensmith: 0000-0001-6400-8106

Author Contributions

#M.D. and A.F.M. contributed equally to this manuscript. All authors have given approval to the final version of the manuscript. M.D., A.F.M., and J.J.G. designed and conducted the experiments; A.F.M. and A.D.S. helped with MRI studies; Z.C. conducted the cell imaging experiments. M.D., P.M.P., and B.S.P. conducted EPR studies; R.P.W. and S.L. performed TEM imaging; R.P.W. synthesized some precursor compounds. M.A.L. helped with TMV isolations. All authors provided edits to the final manuscript.

Notes

The authors declare no competing financial interest.

ACKNOWLEDGMENTS

We thank Dr. Stefanie D. Boyd, Dr. Li Liu, and Dr. Duane D. Winkler for providing assistance with the fluorescent gels. J.J.G. acknowledges the National Science foundation (DMR-1654405) and the Cancer Prevention and Research Institute of Texas (CPRIT) (RP170752) for their support. A.D.S acknowledges support from the Robert A. Welch Foundation (AT-584). B.S.P. acknowledges the National Institute of Health (NIGMS, GM117511-01-01) and the National Science Foundation (CHE, 1709369).

REFERENCES

(1) Bakalova, R.; Georgieva, E.; Ivanova, D.; Zhelev, Z.; Aoki, I.; Saga, T. Magnetic Resonance Imaging of Mitochondrial Dysfunction and Metabolic Activity, Accompanied by Overproduction of Superoxide. *ACS Chem. Neurosci.* **2015**, *6* (12), 1922−1929.

(2) Sabharwal, S. S.; Schumacker, P. T. Mitochondrial ROS in cancer: initiators, amplifiers or an Achilles' heel? *Nat. Rev. Cancer* **2014**, *14* (11), 709−721.

(3) Desideri, E.; Vegliante, R.; Ciriolo, M. R. Mitochondrial dysfunctions in cancer: Genetic defects and oncogenic signaling impinging on TCA cycle activity. *Cancer Lett.* **2015**, *356* (2), 217−223.

(4) Pinto, M.; Moraes, C. T. Mitochondrial genome changes and neurodegenerative diseases. *Biochim. Biophys. Acta, Mol. Basis Dis.* **2014**, *1842* (8), 1198−1207.

(5) Yadav, A.; Agarwal, S.; Tiwari, S.; Chaturvedi, R. Mitochondria: Prospective Targets for Neuroprotection in Parkinson's Disease. *Curr. Pharm. Des.* **2014**, *20* (35), 5558−5573.

(6) Giacco, F.; Brownlee, M. Oxidative stress and diabetic complications. *Circ. Res.* **2010**, *107* (9), 1058−1070.

(7) Lowell, B. B.; Shulman, G. I. Mitochondrial dysfunction and type 2 diabetes. *Science* **2005**, *307* (5708), 384−387.

(8) Campuzano, V.; Montermini, L.; Molto, M. D.; Pianese, L.; Cossee, M.; Cavalcanti, F.; Monros, E.; Rodius, F.; Duclos, F.; Monticelli, A.; Zara, F.; Canizares, J.; Koutnikova, H.; Bidichandani, S. I.; Gellera, C.; Brice, A.; Trouillas, P.; De Michele, G.; Filla, A.; De Frutos, R.; Palau, F.; Patel, P. I.; Di Donato, S.; Mandel, J. L.; Cocozza, S.; Koenig, M.; Pandolfo, M. Friedreich's Ataxia: Autosomal Recessive Disease Caused by an Intronic GAA Triplet Repeat Expansion. *Science* **1996**, *271* (5254), 1423−1427.

DOI: 10.1021/acs.molpharmaceut.8b00262
Mol. Pharmaceutics 2018, 15, 2973−2983

(9) Mascialino, B.; Leinonen, M.; Meier, T. Meta-analysis of the prevalence of Leber hereditary optic neuropathy mtDNA mutations in Europe. *Eur. J.Ophthalmol.* **2012**, *22* (3), 461−465.
(10) Montagna, P.; Gallassi, R.; Medori, R.; Govoni, E.; Zeviani, M.; Di Mauro, S.; Lugaresi, E.; Andermann, F. MELAS syndrome: characteristic migrainous and epileptic features and maternal transmission. *Neurology* **1988**, *38* (5), 751.
(11) Wallace, D. C.; Zheng, X.; Lott, M. T.; Shoffner, J. M.; Hodge, J. A.; Kelley, R. I.; Epstein, C. M.; Hopkins, L. C. Familial mitochondrial encephalomyopathy (MERRF): Genetic, pathophysiological, and biochemical characterization of a mitochondrial DNA disease. *Cell* **1988**, *55* (4), 601−610.
(12) Hayashi, G.; Cortopassi, G. Oxidative stress in inherited mitochondrial diseases. *Free Radical Biol. Med.* **2015**, *88* (Pt A), 10−17.
(13) Rahman, S.; Blok, R. B.; Dahl, H. H.; Danks, D. M.; Kirby, D. M.; Chow, C. W.; Christodoulou, J.; Thorburn, D. R. Leigh syndrome: clinical features and biochemical and DNA abnormalities. *Ann. Neurol.* **1996**, *39* (3), 343−351.
(14) Abbas, K.; Hardy, M.; Poulhes, F.; Karoui, H.; Tordo, P.; Ouari, O.; Peyrot, F. Detection of superoxide production in stimulated and unstimulated living cells using new cyclic nitrone spin traps. *Free Radical Biol. Med.* **2014**, *71*, 281−290.
(15) Mrakic-Sposta, S.; Gussoni, M.; Montorsi, M.; Porcelli, S.; Vezzoli, A. Assessment of a standardized ROS production profile in humans by electron paramagnetic resonance. *Oxid. Med. Cell. Longevity* **2012**, *2012*, 973927.
(16) Krotz, F.; Sohn, H. Y.; Pohl, U. Reactive oxygen species: players in the platelet game. *Arterioscler., Thromb., Vasc. Biol.* **2004**, *24* (11), 1988−1996.
(17) Apel, K.; Hirt, H. Reactive oxygen species: metabolism, oxidative stress, and signal transduction. *Annu. Rev. Plant Biol.* **2004**, *55*, 373−399.
(18) Kanofsky, J. R. Singlet oxygen production by biological systems. *Chem.-Biol. Interact.* **1989**, *70* (1−2), 1−28.
(19) Kayama, Y.; Raaz, U.; Jagger, A.; Adam, M.; Schellinger, I. N.; Sakamoto, M.; Suzuki, H.; Toyama, K.; Spin, J. M.; Tsao, P. S. Diabetic Cardiovascular Disease Induced by Oxidative Stress. *Int. J. Mol. Sci.* **2015**, *16* (10), 25234−25263.
(20) Cai, L.; Wang, J.; Li, Y.; Sun, X.; Wang, L.; Zhou, Z.; Kang, Y. J. Inhibition of Superoxide Generation and Associated Nitrosative-Damage Is Involved in Metallothionein Prevention of Diabetic Cardiomyopathy. *Diabetes* **2005**, *54* (6), 1829−1837.
(21) Woods, M.; Woessner, D. E.; Sherry, A. D. Paramagnetic lanthanide complexes as PARACEST agents for medical imaging. *Chem. Soc. Rev.* **2006**, *35* (6), 500−511.
(22) Viswanathan, S.; Kovacs, Z.; Green, K. N.; Ratnakar, S. J.; Sherry, A. D. Alternatives to gadolinium-based metal chelates for magnetic resonance imaging. *Chem. Rev.* **2010**, *110* (5), 2960−3018.
(23) Sherry, A. D.; Woods, M. Chemical exchange saturation transfer contrast agents for magnetic resonance imaging. *Annu. Rev. Biomed. Eng.* **2008**, *10*, 391−411.
(24) Spasojević, I. Electron Paramagnetic Resonance - A Powerful Tool of Medical Biochemistry in Discovering Mechanisms of Disease and Treatment Prospects. *J. Med. Biochem.* **2010**, *29*, 175−188.
(25) Ratnakar, S. J.; Soesbe, T. C.; Lumata, L. L.; Do, Q. N.; Viswanathan, S.; Lin, C. Y.; Sherry, A. D.; Kovacs, Z. Modulation of CEST images in vivo by T_1 relaxation: a new approach in the design of responsive PARACEST agents. *J. Am. Chem. Soc.* **2013**, *135* (40), 14904−14907.
(26) Zhang, L.; Martins, A. F.; Zhao, P.; Wu, Y.; Tircso, G.; Sherry, D. Lanthanide-based T_{2ex} and CEST complexes provide new insights into the design of pH sensitive MRI agents. *Angew. Chem., Int. Ed.* **2017**, *56*, 16626−16630.
(27) Zhang, L.; Martins, A. F.; Mai, Y. Y.; Zhao, P. Y.; Funk, A. M.; Clavijo Jordan, M. V. C.; Zhang, S. R.; Chen, W.; Wu, Y. K.; Sherry, A. D. Imaging Extracellular Lactate In Vitro and In Vivo Using CEST MRI and a Paramagnetic Shift Reagent. *Chem. - Eur. J.* **2017**, *23*, 1752−1756.
(28) Song, B.; Wu, Y.; Yu, M.; Zhao, P.; Zhou, C.; Kiefer, G. E.; Sherry, A. D. A europium(III)-based PARACEST agent for sensing singlet oxygen by MRI. *Dalton Trans.* **2013**, *42*, 8066−8069.
(29) Do, Q. N.; Ratnakar, J. S.; Kovacs, Z.; Sherry, A. D. Redox- and hypoxia-responsive MRI contrast agents. *ChemMedChem* **2014**, *9*, 1116−1129.
(30) Hyodo, F.; Matsumoto, K.; Matsumoto, A.; Mitchell, J. B.; Krishna, M. C. Probing the intracellular redox status of tumors with magnetic resonance imaging and redox-sensitive contrast agents. *Cancer Res.* **2006**, *66*, 9921−9928.
(31) Prescott, C.; Bottle, S. E. Biological Relevance of Free Radicals and Nitroxides. *Cell Biochem. Biophys.* **2017**, *75*, 227−240.
(32) Liu, S. J.; Zhou, N.; Chen, Z. J.; Wei, H. J.; Zhu, Y. N.; Guo, S.; Zhao, Q. Using a redox-sensitive phosphorescent probe for optical evaluation of an intracellular redox environment. *Opt. Lett.* **2017**, *42*, 13−16.
(33) Sowers, M. A.; McCombs, J. R.; Wang, Y.; Paletta, J. T.; Morton, S. W.; Dreaden, E. C.; Boska, M. D.; Ottaviani, M. F.; Hammond, P. T.; Rajca, A.; Johnson, J. A. Redox-responsive branched-bottlebrush polymers for in vivo MRI and fluorescence imaging. *Nat. Commun.* **2014**, *5*, 5460.
(34) Merbach, A.; Helm, L.; Toth, E. *The Chemistry of Contrast Agents in Medical Magnetic Resonance Imaging*, 2nd ed.; John Wiley & Sons, 2013.
(35) Nguyen, H. V.; Chen, Q.; Paletta, J. T.; Harvey, P.; Jiang, Y.; Zhang, H.; Boska, M. D.; Ottaviani, M. F.; Jasanoff, A.; Rajca, A.; Johnson, J. A. Nitroxide-Based Macromolecular Contrast Agents with Unprecedented Transverse Relaxivity and Stability for Magnetic Resonance Imaging of Tumors. *ACS Cent. Sci.* **2017**, *3* (7), 800−811.
(36) Garmendia, S.; Mantione, D.; Alonso-de Castro, S.; Jehanno, C.; Lezama, L.; Hedrick, J. L.; Mecerreyes, D.; Salassa, L.; Sardon, H. Polyurethane based organic macromolecular contrast agents (PU-ORCAs) for magnetic resonance imaging. *Polym. Chem.* **2017**, *8* (17), 2693−2701.
(37) Chan, J. M. W.; Wojtecki, R. J.; Sardon, H.; Lee, A. L. Z.; Smith, C. E.; Shkumatov, A.; Gao, S. J.; Kong, H.; Yang, Y. Y.; Hedrick, J. L. Self-Assembled, Biodegradable Magnetic Resonance Imaging Agents: Organic Radical-Functionalized Diblock Copolymers. *ACS Macro Lett.* **2017**, *6* (2), 176−180.
(38) Haugland, M. M.; Anderson, E. A.; Lovett, J. E. *Tuning the properties of nitroxide spin labels for use in electron paramagnetic resonance spectroscopy through chemical modification of the nitroxide framework* **2016**, *25*, 1−34.
(39) Rajca, A.; Wang, Y.; Boska, M.; Paletta, J. T.; Olankitwanit, A.; Swanson, M. A.; Mitchell, D. G.; Eaton, S. S.; Eaton, G. R.; Rajca, S. Organic radical contrast agents for magnetic resonance imaging. *J. Am. Chem. Soc.* **2012**, *134* (38), 15724−15727.
(40) Yamada, K.; Mito, F.; Matsuoka, Y.; Ide, S.; Shikimachi, K.; Fujiki, A.; Kusakabe, D.; Ishida, Y.; Enoki, M.; Tada, A.; Ariyoshi, M.; Yamasaki, T.; Yamato, M. Fluorescence probes to detect lipid-derived radicals. *Nat. Chem. Biol.* **2016**, *12* (8), 608−613.
(41) Anderson, E. A.; Isaacman, S.; Peabody, D. S.; Wang, E. Y.; Canary, J. W.; Kirshenbaum, K. Viral nanoparticles donning a paramagnetic coat: conjugation of MRI contrast agents to the MS2 capsid. *Nano Lett.* **2006**, *6* (6), 1160−1164.
(42) Chen, Z.; Li, N.; Li, S.; Dharmarwardana, M.; Schlimme, A.; Gassensmith, J. J. Viral chemistry: the chemical functionalization of viral architectures to create new technology. *WIREs Nanomed. Nanobiotechnol.* **2016**, *8* (4), 512−534.
(43) Scholthof, K. B.; Adkins, S.; Czosnek, H.; Palukaitis, P.; Jacquot, E.; Hohn, T.; Hohn, B.; Saunders, K.; Candresse, T.; Ahlquist, P.; Hemenway, C.; Foster, G. D. Top 10 plant viruses in molecular plant pathology. *Mol. Plant Pathol.* **2011**, *12* (9), 938−954.
(44) Harrison, B. D.; Wilson, T. M. Milestones in the research on tobacco mosaic virus. *Philos. Trans. R. Soc., B* **1999**, *354* (1383), 521−529.
(45) Klug, A. The tobacco mosaic virus particle: structure and assembly. *Philos. Trans. R. Soc., B* **1999**, *354* (1383), 531−535.

DOI: 10.1021/acs.molpharmaceut.8b00262
Mol. Pharmaceutics 2018, 15, 2973−2983

(46) Sitasuwan, P.; Lee, L. A.; Li, K.; Nguyen, H. G.; Wang, Q. RGD-conjugated rod-like viral nanoparticles on 2D scaffold improve bone differentiation of mesenchymal stem cells. *Front. Chem.* **2014**, *2*, 31.
(47) Miller, R. A.; Stephanopoulos, N.; McFarland, J. M.; Rosko, A. S.; Geissler, P. L.; Francis, M. B. Impact of Assembly State on the Defect Tolerance of TMV-Based Light Harvesting Arrays. *J. Am. Chem. Soc.* **2010**, *132*, 6068−6074.
(48) Datta, A.; Hooker, J. M.; Botta, M.; Francis, M. B.; Aime, S.; Raymond, K. N. High relaxivity gadolinium hydroxypyridonate-viral capsid conjugates: nanosized MRI contrast agents. *J. Am. Chem. Soc.* **2008**, *130* (8), 2546−2552.
(49) Schlick, T. L.; Ding, Z.; Kovacs, E. W.; Francis, M. B. Dual-surface modification of the tobacco mosaic virus. *J. Am. Chem. Soc.* **2005**, *127* (11), 3718−23.
(50) Li, S.; Dharmarwardana, M.; Welch, R. P.; Ren, Y.; Thompson, C. M.; Smaldone, R. A.; Gassensmith, J. J. Template-Directed Synthesis of Porous and Protective Core−Shell Bionanoparticles. *Angew. Chem., Int. Ed.* **2016**, *55* (36), 10691−10696.
(51) Li, S.; Dharmarwardana, M.; Welch, R. P.; Benjamin, C. E.; Shamir, A. M.; Nielsen, S. O.; Gassensmith, J. J. Investigation of Controlled Growth of Metal−Organic Frameworks on Anisotropic Virus Particles. *ACS Appl. Mater. Interfaces* **2018**; Article ASAP.
(52) Bruckman, M. A.; Randolph, L. N.; Gulati, N. M.; Stewart, P. L.; Steinmetz, N. F. Silica-coated Gd(DOTA)-loaded protein nanoparticles enable magnetic resonance imaging of macrophages. *J. Mater. Chem. B* **2015**, *3* (38), 7503−7510.
(53) Bye, N.; Hutt, O. E.; Hinton, T. M.; Acharya, D. P.; Waddington, L. J.; Moffat, B. A.; Wright, D. K.; Wang, H. X.; Mulet, X.; Muir, B. W. Nitroxide-loaded hexosomes provide MRI contrast in vivo. *Langmuir* **2014**, *30* (29), 8898−906.
(54) Hu, H.; Zhang, Y.; Shukla, S.; Gu, Y.; Yu, X.; Steinmetz, N. F. Dysprosium-Modified Tobacco Mosaic Virus Nanoparticles for Ultra-High-Field Magnetic Resonance and Near-Infrared Fluorescence Imaging of Prostate Cancer. *ACS Nano* **2017**, *11* (9), 9249−9258.
(55) Bruckman, M. A.; Hern, S.; Jiang, K.; Flask, C. A.; Yu, X.; Steinmetz, N. F. Tobacco mosaic virus rods and spheres as supramolecular high-relaxivity MRI contrast agents. *J. Mater. Chem. B* **2013**, *1* (10), 1482−1490.
(56) Bruckman, M. A.; Jiang, K.; Simpson, E. J.; Randolph, L. N.; Luyt, L. G.; Yu, X.; Steinmetz, N. F. Dual-modal magnetic resonance and fluorescence imaging of atherosclerotic plaques in vivo using VCAM-1 targeted tobacco mosaic virus. *Nano Lett.* **2014**, *14* (3), 1551−1558.
(57) Prasuhn, D. E., Jr.; Yeh, R. M.; Obenaus, A.; Manchester, M.; Finn, M. G. Viral MRI contrast agents: coordination of Gd by native virions and attachment of Gd complexes by azide-alkyne cycloaddition. *Chem. Commun.* **2007**, *0* (12), 1269−1271.
(58) Liepold, L.; Anderson, S.; Willits, D.; Oltrogge, L.; Frank, J. A.; Douglas, T.; Young, M. Viral capsids as MRI contrast agents. *Magn. Reson. Med.* **2007**, *58* (5), 871−879.
(59) Garimella, P. D.; Datta, A.; Romanini, D. W.; Raymond, K. N.; Francis, M. B. Multivalent, high-relaxivity MRI contrast agents using rigid cysteine-reactive gadolinium complexes. *J. Am. Chem. Soc.* **2011**, *133* (37), 14704−14709.
(60) Hooker, J. M.; Datta, A.; Botta, M.; Raymond, K. N.; Francis, M. B. Magnetic resonance contrast agents from viral capsid shells: a comparison of exterior and interior cargo strategies. *Nano Lett.* **2007**, *7* (8), 2207−2210.
(61) Raymond, K. N.; Pierre, V. C. Next generation, high relaxivity gadolinium MRI agents. *Bioconjugate Chem.* **2005**, *16* (1), 3−8.
(62) Allen, M.; Bulte, J. W.; Liepold, L.; Basu, G.; Zywicke, H. A.; Frank, J. A.; Young, M.; Douglas, T. Paramagnetic viral nanoparticles as potential high-relaxivity magnetic resonance contrast agents. *Magn. Reson. Med.* **2005**, *54* (4), 807−12.
(63) Qazi, S.; Liepold, L. O.; Abedin, M. J.; Johnson, B.; Prevelige, P.; Frank, J. A.; Douglas, T. P22 viral capsids as nanocomposite high-relaxivity MRI contrast agents. *Mol. Pharmaceutics* **2013**, *10* (1), 11−17.
(64) Bruckman, M. A.; Steinmetz, N. F. Chemical modification of the inner and outer surfaces of Tobacco Mosaic Virus (TMV). *Methods Mol. Biol.* **2014**, *1108*, 173−185.
(65) Hong, V.; Presolski, S. I.; Ma, C.; Finn, M. G. Analysis and optimization of copper-catalyzed azide-alkyne cycloaddition for bioconjugation. *Angew. Chem., Int. Ed.* **2009**, *48* (52), 9879−9883.
(66) Bruckman, M. A.; Kaur, G.; Lee, L. A.; Xie, F.; Sepulveda, J.; Breitenkamp, R.; Zhang, X.; Joralemon, M.; Russell, T. P.; Emrick, T.; Wang, Q. Surface modification of tobacco mosaic virus with "click" chemistry. *ChemBioChem* **2008**, *9* (4), 519−523.
(67) Franchi, P.; Lucarini, M.; Pedrielli, P.; Pedulli, G. F. Nitroxide Radicals as Hydrogen Bonding Acceptors. An Infrared and EPR Study. *ChemPhysChem* **2002**, *3* (9), 789−793.
(68) Caravan, P.; Farrar, C. T.; Frullano, L.; Uppal, R. Influence of molecular parameters and increasing magnetic field strength on relaxivity of gadolinium- and manganese-based T_1 contrast agents. *Contrast Media Mol. Imaging* **2009**, *4* (2), 89−100.
(69) Maliakal, A. J.; Turro, N. J.; Bosman, A. W.; Cornel, J.; Meijer, E. W. Relaxivity Studies on Dinitroxide and Polynitroxyl Functionalized Dendrimers: Effect of Electron Exchange and Structure on Paramagnetic Relaxation Enhancement. *J. Phys. Chem. A* **2003**, *107* (41), 8467−8475.
(70) Halle, B.; Wennerström, H. Nearly exponential quadrupolar relaxation. A perturbation treatment. *J. Magn. Reson.* **1981**, *44* (1), 89−100.
(71) The narrowing condition is defined for these systems when one of the two portions of the inner-sphere T_2 and T_1 converge to one of the sides depending on the rate of the proton exchange, T_e, tumbling, and chemical shift that is proportional the magnetic field.
(72) Luchinat, C.; Bertini, I. *NMR of Paramagnetic Molecules in Biological Systems*; Physical Bioinorganic Chemistry Series; Benjamin-Cummings; 1986.
(73) Vander Elst, L.; Roch, A.; Gillis, P.; Laurent, S.; Botteman, F.; Bulte, J. W.; Muller, R. N. Dy-DTPA derivatives as relaxation agents for very high field MRI: the beneficial effect of slow water exchange on the transverse relaxivities. *Magn. Reson. Med.* **2002**, *47* (6), 1121−1130.
(74) Caravan, P.; Greenfield, M. T.; Bulte, J. W. Molecular factors that determine Curie spin relaxation in dysprosium complexes. *Magn. Reson. Med.* **2001**, *46* (5), 917−22.
(75) Swift, T. J.; Connick, R. E. NMR-Relaxation Mechanisms of O17in Aqueous Solutions of Paramagnetic Cations and the Lifetime of Water Molecules in the First Coordination Sphere. *J. Chem. Phys.* **1962**, *37* (2), 307−320.
(76) Bertini, I.; Luchinat, C.; Parigi, G.; Ravera, E. *NMR of Paramagnetic Molecules Applications to Metallobiomolecules and Model*, 2nd ed.; Elsevier: Amsterdam, 2017.
(77) Pereira, G. A.; Ananias, D.; Rocha, J.; Amaral, V. S.; Muller, R. N.; Elst, L. V.; Tóth, É.; Peters, J. A.; Geraldes, C. F. G. C. NMR relaxivity of Ln^{3+}-based zeolite-type materials. *J. Mater. Chem.* **2005**, *15* (35−36), 3832.
(78) Hyodo, F.; Soule, B. P.; Matsumoto, K.; Matusmoto, S.; Cook, J. A.; Hyodo, E.; Sowers, A. L.; Krishna, M. C.; Mitchell, J. B. Assessment of tissue redox status using metabolic responsive contrast agents and magnetic resonance imaging. *J. Pharm. Pharmacol.* **2008**, *60* (8), 1049−1060.
(79) Bobko, A. A.; Kirilyuk, I. A.; Grigor'ev, I. A.; Zweier, J. L.; Khramtsov, V. V. Reversible reduction of nitroxides to hydroxylamines: roles for ascorbate and glutathione. *Free Radical Biol. Med.* **2007**, *42* (3), 404−12.
(80) Sato, S.; Endo, S.; Kurokawa, Y.; Yamaguchi, M.; Nagai, A.; Ito, T.; Ogata, T. Synthesis and fluorescence properties of six fluorescein-nitroxide radical hybrid-compounds. *Spectrochim. Acta, Part A* **2016**, *169*, 66−71.
(81) Shukla, S.; Eber, F. J.; Nagarajan, A. S.; DiFranco, N. A.; Schmidt, N.; Wen, A. M.; Eiben, S.; Twyman, R. M.; Wege, C.; Steinmetz, N. F. The Impact of Aspect Ratio on the Biodistribution and Tumor Homing of Rigid Soft-Matter Nanorods. *Adv. Healthcare Mater.* **2015**, *4* (6), 874−82.

DOI: 10.1021/acs.molpharmaceut.8b00262
Mol. Pharmaceutics 2018, 15, 2973−2983

(82) Liu, X.; Wu, F.; Tian, Y.; Wu, M.; Zhou, Q.; Jiang, S.; Niu, Z. Size Dependent Cellular Uptake of Rod-like Bionanoparticles with Different Aspect Ratios. *Sci. Rep.* **2016**, *6*, 24567.
(83) Dikalov, S. I.; Kirilyuk, I. A.; Voinov, M.; Grigor'ev, I. A. EPR detection of cellular and mitochondrial superoxide using cyclic hydroxylamines. *Free Radical Res.* **2011**, *45* (4), 417−430.
(84) Yapici, N. B.; Jockusch, S.; Moscatelli, A.; Mandalapu, S. R.; Itagaki, Y.; Bates, D. K.; Wiseman, S.; Gibson, K. M.; Turro, N. J.; Bi, L. New rhodamine nitroxide based fluorescent probes for intracellular hydroxyl radical identification in living cells. *Org. Lett.* **2012**, *14* (1), 50−3.
(85) Abbas, K.; Hardy, M.; Poulhes, F.; Karoui, H.; Tordo, P.; Ouari, O.; Peyrot, F. Detection of superoxide production in stimulated and unstimulated living cells using new cyclic nitrone spin traps. *Free Radical Biol. Med.* **2014**, *71*, 281−90.
(86) Fridovich, I. Quantitative Aspects of the Production of Superoxide Anion Radical by Milk Xanthine Oxidase. *J. Biol. Chem.* **1970**, *245*, 4053−4057.
(87) McCord, J. M.; Fridovich, I. The Reduction of Cytochrome c by Milk Xanthine Oxidase. *J. Biol. Chem.* **1968**, *243*, 5753−5760.

DOI: 10.1021/acs.molpharmaceut.8b00262
Mol. Pharmaceutics 2018, 15, 2973−2983